Combustion Science and Technology
Publication details, including instructions for authors and subscription information:
http://www.informaworld.com/smpp/title~content=t713456315

EFFECTS OF ENTRY CONDITIONS ON CRACKED KEROSENE-FUELED SUPERSONIC COMBUSTOR PERFORMANCE

Xuejun Fan[a]; Gong Yu[a]; Jianguo Li[a]; Lianjie Yue[a]; Xinyu Zhang[a]; Chih-Jen Sung[b]
[a] Institute of Mechanics, Chinese Academy of Sciences, Beijing, P. R. China [b] Department of Mechanical and Aerospace Engineering, Case Western Reserve University, Cleveland, Ohio, USA

To cite this Article Fan, Xuejun , Yu, Gong , Li, Jianguo , Yue, Lianjie , Zhang, Xinyu and Sung, Chih-Jen(2007) 'EFFECTS OF ENTRY CONDITIONS ON CRACKED KEROSENE-FUELED SUPERSONIC COMBUSTOR PERFORMANCE', Combustion Science and Technology, 179: 10, 2199 — 2217
To link to this Article: DOI: 10.1080/00102200701386198
URL: http://dx.doi.org/10.1080/00102200701386198

Combust. Sci. and Tech., 179: 2199–2217, 2007

ISSN: 0010-2202 print/1563-521X online
DOI: 10.1080/00102200701386198

Effects of Entry Conditions on Cracked Kerosene-Fueled Supersonic Combustor Performance

Xuejun Fan, Gong Yu, Jianguo Li, Lianjie Yue, and Xinyu Zhang
Institute of Mechanics, Chinese Academy of Sciences, Beijing, P. R. China

Chih-Jen Sung
Department of Mechanical and Aerospace Engineering, Case Western Reserve University, Cleveland, Ohio, USA

Abstract: Supersonic combustion of thermally cracked kerosene was experimentally investigated in two model supersonic combustors with different entry cross-section areas. Effects of entry static pressure, entry Mach number, combustor entry geometry, and injection scheme on combustor performance were systematically investigated and discussed based on the measured static pressure distribution and specific thrust increment due to combustion. In addition, the methodology for characterizing flow rate and composition of cracked kerosene was detailed. Using a pulsed Schlieren system, the interaction of supercritical and cracked kerosene jet plumes with a Mach 2.5 crossflow was also visualized at different injection temperatures. The present experimental results suggest that the use of a higher combustor entry Mach number as well as a larger combustor duct height would suppress the boundary layer separation near the combustor entrance and avoid the problem of inlet un-start.

Received 15 November 2006; accepted 5 March 2007.

Current research program was supported by the National Natural Science Foundation of China under Contractor No. 10232060. The authors would like to acknowledge Prof. X. N. Lu for his assistance in designing and testing the kerosene heater. We also thank Mr. D. X. Qian and Mr. Y. Li for the technical support.

Address correspondence to xfan@imech.ac.cn

Keywords: Entry conditions; Kerosene; Supersonic combustion; Thermal cracking

INTRODUCTION

In practical hydrocarbon-fueled scramjet operations, liquid fuel can be used to cool down the engine flow path and absorb a part of heat imposed by the flight environment. Hence, the fuel state before entering the combustor varies with different operation conditions. When both fuel temperature and pressure are higher than the thermodynamic critical point, the fuel becomes supercritical (Tishkoff et al., 1997; Yang, 2000; Edwards, 2003). Moreover, when the fuel temperature is sufficiently high, thermal decomposition of fuel can occur as well. Since a wide range of fuel states/compositions can exist in the fuel injection system, it is imperative to understand how the changes in fuel property affect the injection behavior and the subsequent combustion processes in supersonic combustors.

To further our understanding of the above important issues, we experimentally investigated the performance of model supersonic combustors with the injection of liquid kerosene (Yu et al., 2001, 2003, 2005a) and vaporized/supercritical kerosene (Fan et al., 2006). The effects of fuel cracking on supersonic combustion characteristics was also explored using a specially designed kerosene heating and delivery system, which can operate up to 920 K at fuel pressure of 5.5 MPa with minimal/negligible fuel coking. Experimental results (Yu et al., 2005b) demonstrated that the overall burning intensity as well as combustion efficiency improved with supercritical/cracked kerosene injection, and generally increased with increasing fuel temperature. It was also noted that the fuel temperature as well as the degree of fuel cracking, rather than the fuel injection pressure, play an important role in affecting the combustor performance.

The present study aims to extend our previous experimental efforts by including thrust measurement with a newly built facility and assessing the effects of entry conditions on combustor performance. A pulsed Schlieren system was also developed for flow visualization. Experimental results to be presented herein include the schlieren images of supercritical/cracked kerosene jet plumes in a Mach 2.5 cross-flow, the effects of fuel injection scheme and entry static pressure/Mach number of airflow on combustor performance, and the performance comparison of model combustors with two different entry cross-sections. The present test facility and its key sub-systems are described here in detail. Current experimental results are presented and discussed.

EXPERIMENTAL SPECIFICATIONS

Test Facility

The test rig consisted of a vitiated air supply system, multi-purpose model supersonic combustors, and a kerosene delivery and heating system. Figure 1 shows the schematic of the model supersonic combustors and different modules of integrated fuel injection and flameholder employed in this study. All of the experimental controls and data acquisitions were accomplished with a computer. The air supply system was capable of supplying heated air at stagnation temperatures of 800–2100 K and stagnation pressures of 0.7–2.5 MPa. It usually took approximately 2.5 sec to establish a steady Mach 2.5 or Mach 3.0 airflow and a typical run lasted around 7 sec.

Experiments were conducted in two model supersonic combustors, No. 1 and No. 2. Both model combustors had the same total length of

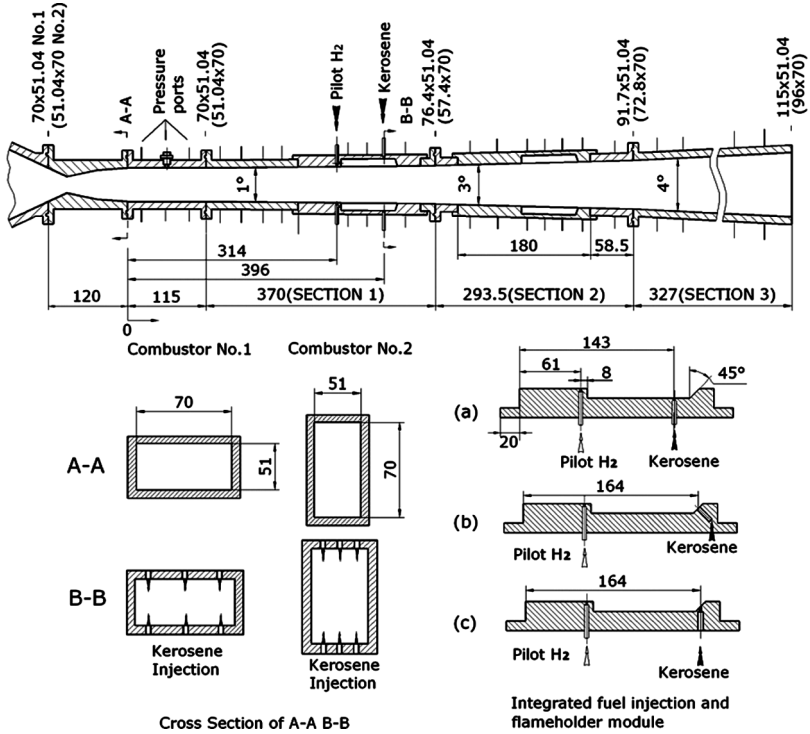

Figure 1. Schematic of kerosene/pilot hydrogen model supersonic combustors and cavity flameholder configurations employed in the present study. All length dimensions are in mm.

1105.5 mm and consisted of a constant area section of 115 mm and three divergent sections of 370, 293.5, and 327 mm with the expansion angles of 1, 3, and 4 degrees, respectively. In Figure 1, the "0" indicated at the beginning of the constant area section represents the origin of all the static pressure distributions to be presented and discussed later. The entry cross section of the combustor No. 1 was 51 mm in height and 70 mm in width, while that of the combustor No. 2 was 70 mm in height and 51 mm in width. To accommodate the differences in entry Mach number and combustor height, four different nozzles were used. For Mach 2.5 airflow, the nozzle throat dimensions were 23.9 mm × 51 mm and 19.8 mm × 70 mm for the combustors No. 1 and No. 2, respectively. For Mach 3.0 airflow, the nozzle throat dimensions of the combustors No. 1 and No. 2 were, respectively, 14.0 mm × 51 mm and 10.3 mm × 70 mm.

Two pairs of interchangeable integrated fuel injector/flameholder cavity modules in tandem were installed on both sides of the combustor, each with a depth of 12 mm, a 45-degree aft ramp angle, and an overall length-to-depth ratio of 7. Although this arrangement of two modules in tandem can be employed for the study of staged fuel injection, kerosene was only injected through the first pair of cavity modules in the present investigations. Three different schemes were used for kerosene injection, as shown in Figure 1. In schemes (a) and (c), kerosene was injected normally to the airflow from the bottom and the rear ramp of the cavity, respectively. In scheme (b), kerosene was injected in the direction normal to the rear ramp. In each scheme, there were nine orifices of 1.0 mm in diameter evenly spaced in spanwise direction for fuel injection. Note that for clarity only three orifices were highlighted in Figure 1. Following the study of Yu et al. (2001), a small amount of pilot hydrogen was used to facilitate the self-ignition of kerosene in the supersonic combustor. There were five orifices of 1.0 mm in diameter available for pilot hydrogen injection. The pilot hydrogen of room temperature was injected normally to the airflow just upstream of the first pair of cavities. The typical equivalence ratio of pilot hydrogen used in this study was 0.07.

For light access and observation, a pair of quartz windows with 66 mm in height and 120 mm in length were installed on both sides of the combustor near the location of the first cavity module pair. It is also noted that in the visualization experiments of jet–crossflow interaction, only a single hole of 1.2 mm in diameter was used for fuel injection.

The entire test rig was mounted upright on a platform as shown in Figure 2. Three weight sensors (Shanghai TM, Model No. NS-TH3), equilaterally spaced and connected in series, were used to support the platform and measure the thrust changes during the experiments. This system yielded a maximum force reading of 7500 N with an uncertainty of 0.2%. Figure 3 shows a typical time history of the thrust signal for a single run. The airflow started up at the point "a". Subsequently, the

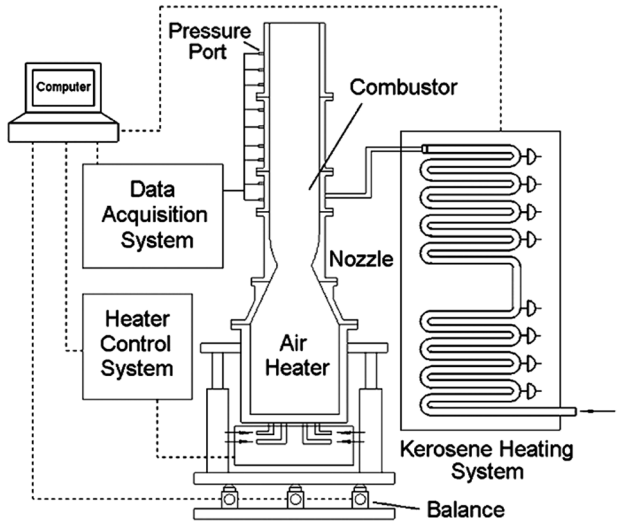

Figure 2. Schematic of test facility with thrust measurement system.

thrust was seen to increase rapidly and level off within one second. Fuel injection then began at the point "b". The thrust level further increased due to the fuel injection and the subsequent supersonic combustion of fuel, and quickly stabilized at the point "c". After a certain experimental duration, the fuel injection was shut off at the point "d" and the thrust

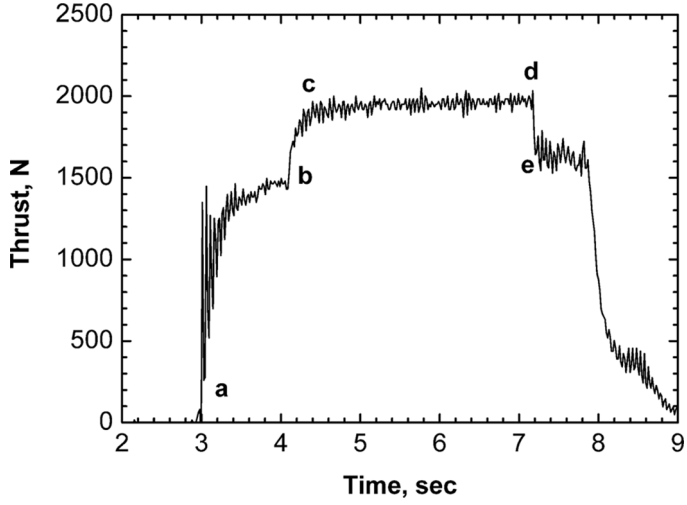

Figure 3. Typical time history of thrust value during experiment.

quickly dropped to the point "e". It is seen from Figure 3 that the thrust increased very slightly from the point "c" to the point "d" because of the time required establishing thermal equilibrium between the core flow and the combustor walls. Nevertheless, the nearly constant thrust level between the points "c" and "d" demonstrates the steadiness of the resulting supersonic combustion and the adequacy of the present test facility. It is also noted that after the kerosene shut off, the point "e" had a slightly higher thrust than the point "b". This is because it took approximately one half second to completely close the fuel valve. The thrust increment as a result of fuel injection and combustion is then defined as the thrust increase from the value at the point "b" to the average value between the points "c" and "d". This thrust increment will be later used as one target parameter for the combustor performance assessment. We further note that if the combustion efficiency is the same, the use of injection scheme (b) is expected to yield a lower thrust because the streamwise component of the fuel injection momentum is opposite to the direction of the core flow.

Kerosene Delivery and Heating System

To minimize the fuel coking at high temperatures, a two-stage heating system as shown in Figure 4 was developed for the present experiments.

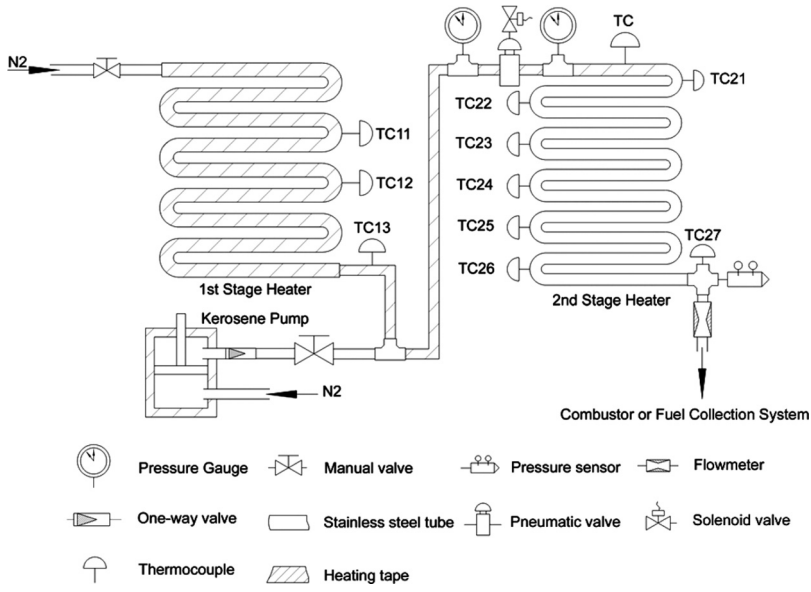

Figure 4. Schematic of two-stage kerosene heating and delivery system.

The first stage was a storage type heater that can heat 0.8 kg kerosene up to 570 K in approximately 10 minutes with negligible coking deposits; while the second stage was a continuous type, which was capable of rapidly heating kerosene to 920 K or higher. The residence time of heated kerosene within the second-stage heater was typically less than 4 seconds, thereby minimizing the extent of fuel coking.

Prior to each experiment the kerosene in a storage cylinder was pumped into the first-stage heater by a piston. Two pneumatic valves (Swagelok, Model No. SS6UM and SS10UM) installed respectively at the exits of the first- and second-stage heaters were employed to turn on/off the two heaters sequentially, as shown in Figure 4. When kerosene in the first-stage heater reached a desired temperature at a given high pressure, kerosene was pressed into the second-stage heater and heated up to the working temperature before injected into the combustor. Two groups of K-type thermocouples (Omega, Model No. KMQSS-0.032E), TC11–13 and TC21–26 in Figure 4, which were installed on the surface of or inserted into the heater tubes, were used to monitor and achieve the feedback control of fuel temperature distribution along the heating system. Stable fuel temperature and pressure at the exit of the heating system were accomplished and maintained during the experiments.

Flow Rate Calibration System

Our previous investigations (Yu et al., 2005b; Fan et al., 2006) demonstrated that the flow rates of supercritical and cracked kerosene can be metered by using a sonic nozzle as long as there is no condensation during flow acceleration and the sonic condition is maintained at the nozzle throat. Figure 5 shows the schematic of the present system for product collection and flow rate calibration. The mass flow rate of supercritical or cracked kerosene was measured using a sonic nozzle installed at the exit of the second-stage heater. The cracked fuel mixture was cooled to room temperature using an air-conditioner condenser circulated with chilled water. The liquid products and minute carbon deposits (if present) were collected after cooling, while the gaseous products were collected using a container immersed in a water pool and the gas mixture volume was measured by the volume of water displaced. The composition of the gas mixture collected was further analyzed using gas chromatography, and its average molecular weight and density were also determined. The mass flow rate of the cracked fuel was determined based on the total mass of the collected liquid and gaseous products over the time duration of fuel discharging. Due to the significant change of the fuel density in the

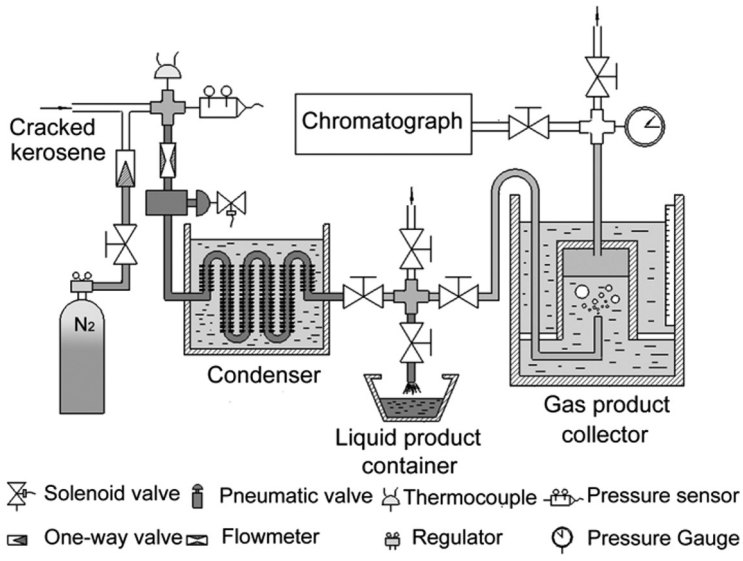

Figure 5. Schematic of a system for flow-rate calibration and gaseous products collection/analysis.

temperature range of 550–920 K, 4 different sonic nozzles with throat diameters of 2.15, 2.5, 3.08, and 3.4 mm were employed in order to cover the flow rate range tested.

Figure 6 shows the calibration results of mass flow rate per unit throat area (Q/S^*) for a fuel pressure of 3.5 MPa in the fuel temperature range of 650–950 K. Calculated results using the NIST SUPERTRAPP (Ely and Huber, 1990) based on a three-species surrogate for the China No. 3 kerosene along with a discharge coefficient of 0.91 for all the sonic nozzles are also plotted for comparison. This three-species surrogate was based on the model proposed by Dagaut (2002) and was developed in our earlier investigation (Fan et al., 2006), consisting by mole of 63% n-dodecane, 30% 1,3,5-trimethylcyclohexane, and 7% n-propylbenzene. It is seen from Figure 6 that below approximately 820 K the calculated values agree well with the experimental data. For fuel temperature higher than 820 K, a large discrepancy is noted, which indicates the significant extent of kerosene cracking beyond this critical temperature. In fact, composition analysis showed that approximately 8% (by weight) of kerosene was cracked at $\sim$860 K fuel temperature in the present setup. Table 1 further lists the measured compositions of gaseous hydrocarbons at four different fuel temperatures using a gas chromatography.

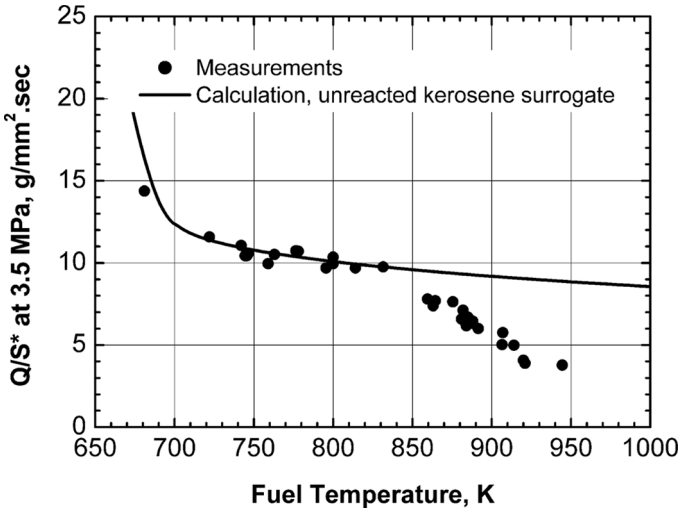

Figure 6. Comparison of measured fuel mass flow rates per unit throat area and calculated values based on a kerosene surrogate at varying fuel temperatures. The fuel pressure is kept constant at 3.5 MPa.

Pulsed Schlieren Visualization System

Instantaneous imaging of the supercritical and cracked kerosene jets into a supersonic crossflow was carried out using a pulsed Schlieren system. An arc discharge with a pulse width of 0.8 μs was utilized as a light source, while a continuous tungsten halogen lamp was also used for alignment. Two reflecting mirrors with 150 mm diameter and 1500 mm focal length were used in the Schlieren setup. The slit width was set to 0.2 mm and the knife-edge was parallel to the longer side of the rectangular image of the slit. Instantaneous schlieren images were recorded on 667 Polaroid films.

Table 1. Molar percentage of gaseous products resulted from thermal cracking of China No. 3 kerosene

Fuel temperature, T_f (K)	Methane CH_4	Ethane C_2H_6	Ethylene C_2H_4	Propane C_3H_8	Propylene C_3H_6	Others C_4–C_5
823	13.72	20.44	18.15	16.78	19.60	11.31
873	21.07	23.62	22.40	13.96	14.47	4.48
903	20.46	23.26	14.74	14.83	17.68	9.03
923	26.81	23.34	18.19	11.78	15.04	4.84

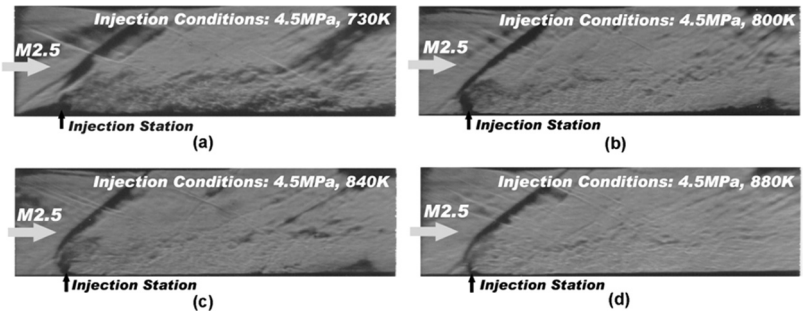

Figure 7. Schlieren images of pressurized fuel jet into a Mach 2.5 crossflow at different injection temperatures. The local airflow static temperature and pressure are 490 K and 0.062 MPa, respectively.

RESULTS AND DISCUSSION

Characterization of Supercritical and Cracked Kerosene Jets into a Supersonic Cross-flow

Figure 7 shows a set of 4 Schlieren images characterizing a single supercritical or cracked kerosene jet into Mach 2.5 airflow in the combustor No. 1. The airflow conditions were kept almost identical in all the experiments, i.e., a static pressure of 0.062 MPa and a static temperature of 490 K. The fuel temperature varied from 730 K to 880 K, while the fuel pressure was kept constant at 4.5 MPa. In the above temperature range, the fuel state varied from supercritical kerosene to partially cracked kerosene (cf. Figure 6).

Similar to our previous kerosene jet structure results in the injection temperature range of 290–550 K (Fan et al., 2006), a bent bow shock upstream of the kerosene jet is visible. Although the China No. 3 kerosene would be in vapor state under the combustor conditions of 0.062 MPa and 490 K, kerosene condensation can still occur in the vicinity of injector where the fuel pressure is much higher than the ambient value, because the corresponding dew point temperature could be equal to or higher than 490 K. As a result, near the injector exit a dark region, which is related to the partial fuel condensation, can be noticed in Figure 7. The size of this dark region is also seen to decrease with increasing fuel injection temperature, indicating reduced amount of fuel condensation. Furthermore, it is noted from Figure 7 that the jet plume appears to be more ''transparent'' as the fuel injection temperature is increased because of diminishing density difference between fuel mixture and air when fuel state varies from supercritical kerosene to partially cracked kerosene. Figure 7 also demonstrates that the jet penetration distance

is not affected much by the reduced fuel mixture density as a result of kerosene cracking.

Reproducibility of Experimental Results

The reproducibility of the experiment data was examined in the combustor No. 1 under approximately identical airflow and fuel injection conditions. Figure 8 shows the static pressure profiles measured from 4 different runs. The fuel flow rates and injection temperatures were kept constant at $\sim 36\,g/s$ and $\sim 890\,K$, respectively. The closeness of the curves shown in Figure 8 demonstrates that the results were highly repeatable. The overall uncertainty in the static pressure measurements from different runs was determined to be within 3%.

Effect of Entry Static Pressure on Combustor Performance

The experiments with varying entry static pressures were conducted in the combustors No. 2 at a fixed entry Mach number 3.0. The fuel was injected at approximately 865 K, and the overall kerosene equivalent

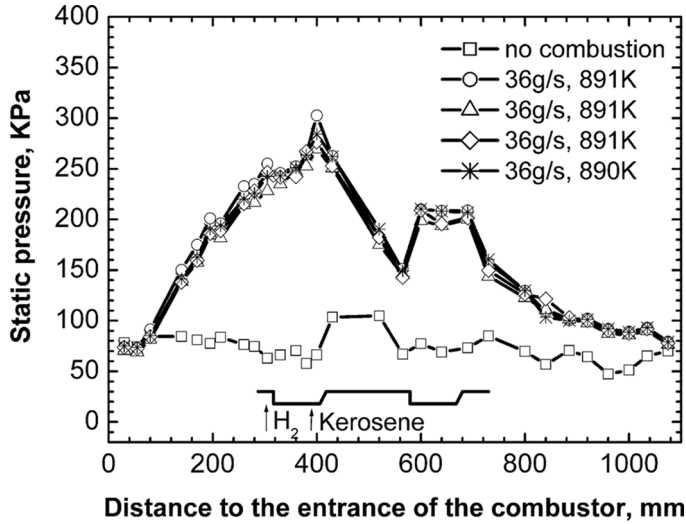

Figure 8. Comparison of static pressure distributions from four different runs in the model combustor No. 1 under approximately identical airflow and fuel injection conditions. Vitiated Mach 2.5 air: stagnation temperature was $\sim 1720\,K$ and stagnation pressure was $\sim 1.11\,MPa$.

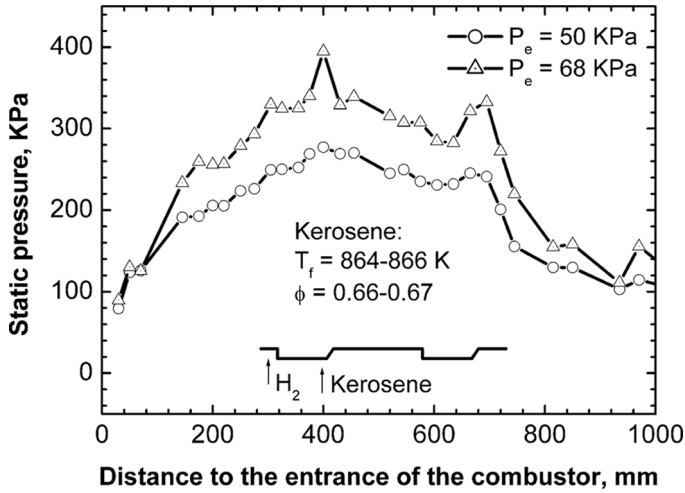

Figure 9. Comparison of static pressure distributions at entry static pressures of 50 and 68 KPa in the model combustor No. 2. Vitiated Mach 3.0 air: stagnation temperature was 1816–1830 K and stagnation pressure was 1.95–2.59 MPa.

ratio of $\sim$0.66 was studied. Combustor configuration with 2 cavities in tandem was utilized, and the fuel was injected from the bottom of the upstream cavity, namely the module (a) shown in Figure 1.

Figure 9 compares the static pressure distributions for two different entry static pressures, $P_e = 50$ and 68 KPa. With a fixed entry Mach number of 3.0, the overall static pressure profiles were seen to be higher for higher entry static pressure. Table 2 lists the measured thrust increment per unit mass flow rate of air ($\mathbf{\Gamma}$) for the conditions of Figure 9 and all other experiments conducted herein. In this comparison, when the entry static pressure was increased from 50 to 68 KPa, the measured $\mathbf{\Gamma}$ increased from 294 m/s to 333 m/s. Note that for a fixed-entry Mach number, a higher entry static pressure implies a higher air mass flow rate, thereby leading to a higher thrust. However, the increase of air specific thruster increment $\mathbf{\Gamma}$ suggests that the overall burning is also enhanced as P_e is increased.

Effect of Injection Scheme on Combustor Performance

Figure 10 compares the static pressure distributions in the combustor No. 1 with 3 different injection schemes – (a), (b), and (c) shown in Figure 1. The fuel and airflow conditions were kept approximately the same in all cases. The corresponding values of $\mathbf{\Gamma}$ are also listed in

Table 2. Experimental conditions and comparison of the experimental and calculated thrust increments per unit air mass flow rate

	Air					Kerosene			Γ		
Fig.	P_0 (MPa)	T_0 (K)	M	Comb. /h (mm)	P_e (MPa)	P_f (MPa)	T_f (K)	ϕ	Exp. (m/s)	Cal. (m/s)	Injection scheme
9	1.95	1816	3.0	No.2/70	0.050	5.05	866	0.67	294	235	a
	2.59	1830	3.0	No.2/70	0.068	3.92	864	0.66	333	314	a
10	1.10	1748	2.5	No.1/51	0.064	3.85	866	0.67	402	470	a
	1.17	1886	2.5	No.1/51	0.067	3.60	857	0.62	363	451	b
	1.12	1823	2.5	No.1/51	0.065	3.86	864	0.67	392	461	c
11	2.54	1848	3.0	No.1/51	0.066	3.76	866	0.64	333	363	a
	1.12	1823	2.5	No.1/51	0.064	3.86	864	0.67	392	437	a
12	2.6	1839	3.0	No.2/70	0.068	3.98	851	0.66	333	323	a
	1.14	1885	2.5	No.2/70	0.066	5.03	864	0.67	343	314	a
13	1.11	1811	2.5	No.2/70	0.064	3.84	869	0.50	274	206	a
	1.11	1628	2.5	No.1/51	0.064	4.98	870	0.49	274	294	a
14	2.44	1617	3.0	No.2/70	0.064	5.08	869	0.49	228	217	a
	2.54	1862	3.0	No.1/51	0.066	4.96	865	0.49	240	242	a

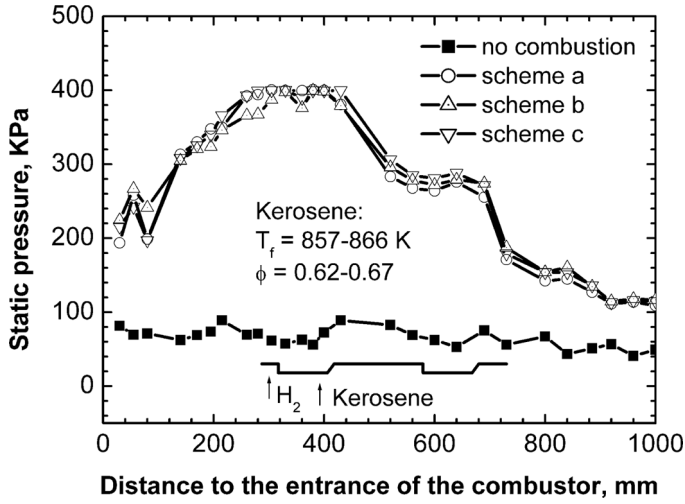

Figure 10. Comparison of static pressure distributions with different fuel injection schemes in the model combustor No. 1. Vitiated Mach 2.5 air: stagnation temperature was 1748–1886 K and stagnation pressure was 1.10–1.17 MPa.

Table 2. It was found that although the static pressure distributions for all three schemes plotted in Figure 10 were similar, the measured specific thrust increment for the scheme (b) was lower than the other two. This lower value of Γ in the scheme (b) could be because the streamwise component of the fuel jet momentum was opposed to the flow direction.

Effect of Entry Mach Number on Combustor Performance

The experiments were conducted in the combustor No. 1 with entry Mach numbers of 2.5 and 3.0. For this comparison, the entry static pressure of the supersonic airflow was kept the same. As such, the total pressure as well as the flow rate required for the Mach 3.0 case is higher than those for the Mach 2.5 case.

Figure 11 compares the effect of entry Mach number (M) on the static pressure distributions in the combustor No. 1 with kerosene equivalent ratios of 0.64–0.67. Again, the corresponding values of Γ are shown in Table 2. It is seen that despite of the similar non-reacting pressure distributions, with combustion the overall pressure rises and the air specific thrust increments in the Mach 2.5 case are higher than those in the Mach 3.0 case. However, in the Mach 2.5 case the pressure rise in the combustor due to excessive heat release caused boundary layer separation, and hence led to a higher back-pressure near the combustor entrance.

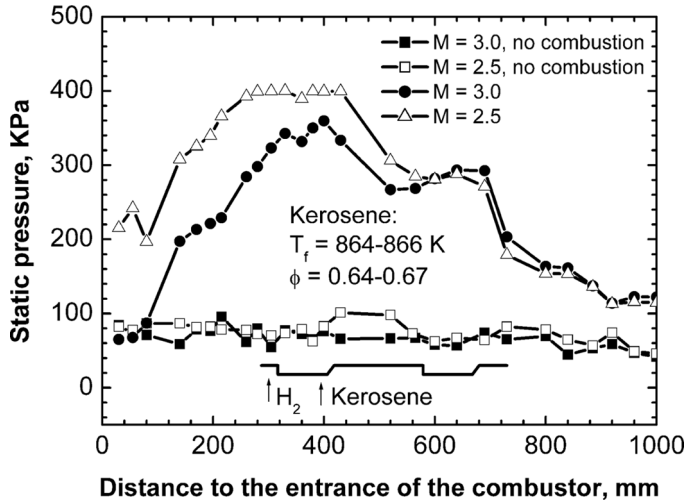

Figure 11. Comparison of static pressure distributions at different entry Mach numbers in the model combustor No. 1. Vitiated Mach 2.5 air: stagnation temperature was 1823 K and stagnation pressure was 1.12 MPa. Vitiated Mach 3.0 air: stagnation temperature was 1848 K and stagnation pressure was 2.54 MPa.

Note that this entry pressure rise could cause an inlet un-start. The present results therefore show that kerosene combustion in the Mach 2.5 airflow is more susceptible to boundary layer separation than in the Mach 3.0 airflow.

Similar test conditions were also conducted in the combustor No. 2 with a larger entrance height of 70 mm. The results are plotted in Figure 12. Since the non-reacting pressure distributions are similar, as seen in Figure 11, only one distribution is shown in Figure 12 as a reference. In contrast to Figure 11, with combustion the difference in static pressure distributions for the 2 entry Mach numbers was much smaller in Figure 12 and no upstream-propagation of combustor pressure wave was noted. These results suggest that increasing combustor entrance height could suppress the boundary separation. Furthermore, for the Mach 3.0 cases the measured values of Γ listed in Table 2 for Figures 11 and 12 are close to each other, even when the combustor entrance height was increased from 51 mm to 70 mm.

Effect of Entrance Height on Combustor Performance

The effect of combustor entrance height on combustor performance was further investigated at a fixed entry Mach number of 2.5. Comparison of the measured static pressure profiles with kerosene equivalence ratio of

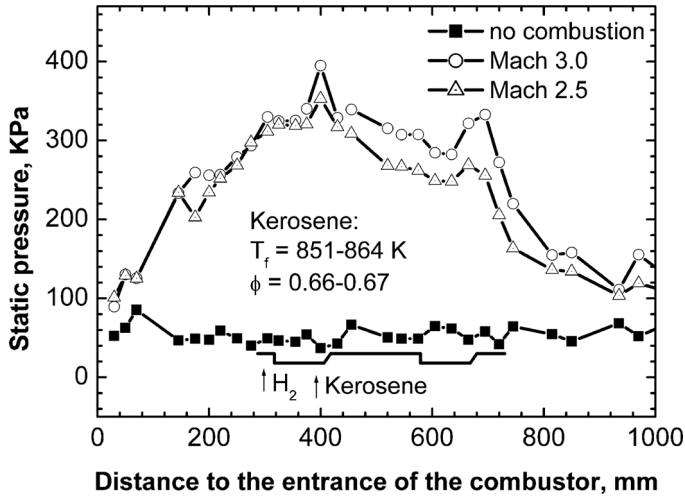

Figure 12. Comparison of static pressure distributions at different entry Mach numbers in the model combustor No. 2. Vitiated Mach 2.5 air: stagnation temperature was 1885 K and stagnation pressure was 1.14 MPa. Vitiated Mach 3.0 air: stagnation temperature was 1839 K and stagnation pressure was 2.60 MPa.

$\sim$0.50 is shown in Figure 13, while the corresponding values of Γ are listed in Table 2. Again, only one non-reacting pressure distribution is plotted in Figure 13 as a reference. Consistent with the findings of

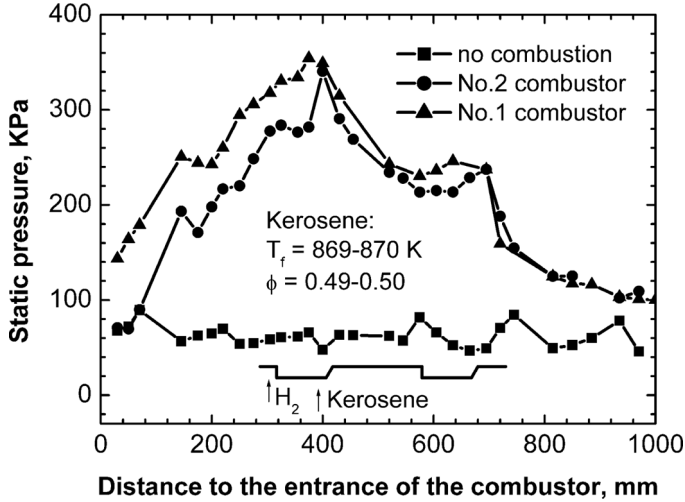

Figure 13. Comparison of static pressure distributions with different model combustors at a fixed entry Mach number of 2.5. Vitiated air: stagnation temperature was 1628–1811 K and stagnation pressure was 1.11 MPa.

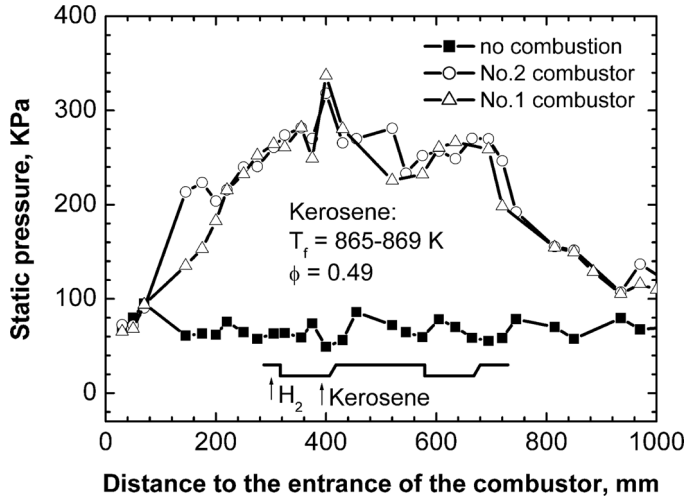

Figure 14. Comparison of static pressure distributions with different model combustors at a fixed entry Mach number of 3.0. Vitiated air: stagnation temperature was 1617–1862 K and stagnation pressure was 2.44–2.54 MPa.

Figures 11 and 12, Figure 13 shows that the static pressures in the combustor No. 1 were higher than those in the combustor No. 2 and the upstream-propagation of pressure waves in the combustor No. 1 occurred even at this leaner equivalent ratio. Therefore, a combustor of larger entrance height, such as the combustor No. 2, seems to be less prone to boundary separation. Recognizing that the change in entrance area can also affect boundary layer separation, future experiments will further investigate the effect of entrance height on combustor performance and boundary separation by keeping the combustor width constant.

Similar experimental conditions as Figure 13 were also conducted with Mach 3.0 entry flow. The corresponding static pressure distributions for the combustors No. 1 and No. 2 are plotted and compared in Figure 14. Unlike the cases with Mach 2.5 entry flow, the pressure rises shown in Figure 14 and the measured specific thrust increments listed in Table 2 for both combustors are seen to be similar, regardless of the difference in entrance height. As demonstrated in Figure 11, the boundary layer separation in the combustor No. 1 is suppressed with increasing Mach number.

Specific Thrust Increment Data

Table 2 summarizes the experiment conditions investigated and the corresponding data of thrust increment per unit air mass flow rate.

With the measured static pressure distribution, the resulting thrust can be calculated based on the streamwise component of the pressure forces acting along the combustor walls. The change in the calculated thrusts before and after combustion is then defined as the thrust increment. The computed values of Γ are also listed in Table 2 and compared with the experimental values. It can be seen from Table 2 that the calculated values of Γ are fairly close to the measured values in most cases, which suggests that the effect of friction on the specific thrust increment is insignificant.

SUMMARY

Combustion of partially cracked kerosene was experimentally studied in two model supersonic combustors. The entry cross section of the combustor No. 1 was 51 mm in height and 70 mm in width, while that of the combustor No. 2 was 70 mm in height and 51 mm in width. Characterization of supercritical/cracked kerosene jets into a Mach 2.5 cross-flow with fuel injection temperature ranging from 730 to 880 K was also carried out using a pulsed Schlieren visualization system. Effects of entry static pressure, entry Mach number, and entry cross-section on combustor performance were studied. Performance assessment was based on the measured static pressure distributions and specific thrust increments. At a fixed entry Mach number, the thrust increment per unit air mass flow rate was found to increase with increasing entry static pressure. Experimental results further demonstrated that ether higher combustor entry Mach number or larger combustor duct height would suppress the boundary layer separation near the combustor entrance and extend the operation range without being affected by inlet un-start.

NOMENCLATURE

h	combustor entrance height
M	Mach number at combustor entrance
P_0	stagnation pressure of airflow
P_e	static pressure at combustor entrance
P_f	stagnation pressure of kerosene
Q	mass flow rate of kerosene
S^*	throat area of sonic nozzle
T_0	stagnation temperature of airflow
T_f	stagnation temperature of kerosene
ϕ	kerosene equivalence ratio
Γ	thrust increment per unit air mass flow rate

REFERENCES

Dagaut, P. (2002) On the kinetics of hydrocarbon oxidation from natural gas to kerosene and diesel fuel. *Phys. Chem. Chem. Phys.*, **4**, 2079–2094.

Edwards, T. (2003) Liquid fuel and propellant for aerospace propulsion: 1903–2003. *J. Propulsion and Power*, **19**(6), 1089–1107.

Ely, J.F. and Huber, M.L. (1990) *NIST Standard Reference Database 4—NIST Thermophysical Properties of Hydrocarbon Mixtures.* National Inst. of Standards, Gaithersburg, MD.

Fan, X.J., Yu, G., Li, J.G., Zhang, X.Y., and Sung, C.J. (2006) Investigation of vaporized kerosene injection and combustion in a supersonic model combustor. *J. Propulsion Power*, **22**(1), 103–110.

Tishkoff, J.M., Drummond, J.P., Edwards, T., and Nejad, A.S. (1997) Future Direction of Supersonic Combustion Research: Air Force/NASA Workshop on Supersonic Combustion. AIAA Paper No. 97-1017.

Yang, V. (2000) Modeling of supercritical vaporization, mixing and combustion processes in liquid-fueled propulsion system. *Proc. Combust. Instit.*, **28**, 925–942.

Yu, G., Fan, X.J., Li, J.G., Yue, L.J., Zhang, X.Y., and Sung, C.J. (2005b) Characterization of a Supersonic Model Combustor with Partially-Cracked Kerosene. AIAA Paper No. 2005-3714.

Yu, G., Li, J.G., Zhang, X.Y., Chen, L.H., and Sung, C.J. (2001) Investigation of kerosene combustion characteristics with pilot hydrogen in model supersonic combustors. *J. Propulsion Power*, **17**(6), 1263–1272.

Yu, G., Li, J.G., Zhang, X.Y., Chen, L.H., and Sung, C.J. (2003) Fuel injection and flame stabilization in a liquid kerosene-fueled supersonic combustor. *J. Propulsion Power*, **19**(5), 885–893.

Yu, G., Li, J.G., Zhao, J.R., Yue, L.J., Chang, X.Y., and Sung, C.J. (2005a) An experimental study of kerosene combustion in a supersonic model combustor using effervescent atomization. *Proc. Combust. Instit.*, **30**, 2859–2866.